2021-05-16

Plant Roots Steer Resilience to Perturbation of River Floodplains

Bau', V

10.1029/2021gl092388
Geophysical Research Letters
American Geophysical Union (AGU)

Supporting Information for "Plant roots steer resilience to perturbation of river floodplains"

Valentina Bau'[1], Alistair G.L. Borthwick [1,2], Paolo Perona[1,3,4]

[1]Institute for Infrastructure and Environment, The University of Edinburgh, Edinburgh EH9 3FG, UK

[2]School of Engineering, Computing and Mathematics, University of Plymouth, Plymouth PL4 8AA, UK

[3]Ecological Engineering Laboratory (ECOL), Institute of Environmental Sciences and Technology (IIE), ENAC Faculty, Ecole Politechnique Federale del Lausanne (EPFL), Lausanne, Switzerland

[4]HOLINGER AG, Urban drainage and hydraulic engineering, Kasthoferstrasse 23, CH-3000 Bern, Switzerland

Contents of this file

Introduction

This Supporting Information provides further information on: the derivation of equations (2) and (4) in the main text, including their context and underlying assumptions; the model parameters used in the case study; and a sensitivity analysis of the effects of

plant elevation η_v, and the tenth D_{10} and ninetieth D_{90} percentiles of the bed sediment grain size distribution on uprooting probability, P_τ, between pre- and post-dam scenarios.

1. Equation for Noise in Erosion process, g_t

Equation 2 in Section 2.1 of the main text expresses random fluctuations in the erosion process, and is used to solve the analytical expression for the probability density function (PDF) of the elapsed time to uprooting p_τ. An expression for the standard deviation of noise characterizing the erosion process, g_t, is derived as follows. Following Perona & Crouzy (2018), we assume that the erosion process can be represented as an Ornstein-Uhlenbeck stochastic process (Uhlenbeck & Ornstein, 1930) involving Gaussian diffusion with drift, where the diffusion coefficient is given by $D(t) = g_t(t)/2$, which, for the sake of simplicity, is assumed constant with respect to time so that $D = g_t/2$. This expression for the diffusion coefficient is well known from Einstein's theory of diffusion (Einstein, 1905) which relates D to the variance σ^2 of the diffusion process after an elapse time t, such that

$$D = \frac{\sigma^2}{2t}. \tag{1}$$

For a discrete random walk process characterized by average jumps (or fluctuations) δ, each taking a time interval $\Delta\tau$ to occur, then, after N steps,

$$D = \frac{N\delta^2}{2N\Delta\tau}. \tag{2}$$

Owing to the scaling properties of the Gaussian diffusion process, the quantity:

$$g_t = 2D = \frac{\delta^2}{\Delta\tau}, \tag{3}$$

is therefore a constant. In order to transpose this idea to a layer of well packed spheres of mean diameter D_{50} (Figure S1), it is necessary to determine an expression that links

the fluctuation time $\Delta\tau$ and fluctuation spatial scale δ to the characteristic quantities of the erosion process. Let us then consider Figure S1, and assume that a turbulent stream flow has a vertical profile of stream-wise velocity component u given by the log-law such that $\frac{\bar{u}}{u_*} = 8.5 + 5.75log(y/k_s)$ (see e.g. Papanicolaou et al. (2002)), where u_* is the bed friction velocity, y is the elevation vertically above the bed, and k_s is the equivalent grain roughness size (here assumed to be equal to the mean sediment size D_{50}). Once an eroded sediment particle of diameter $D_{50} = k_s$ is exposed to the stream flow, then it will travel at a speed that is approximately $\bar{u} = 8.5u_*$ (i.e. as computed from the logarithmic profile for $y = k_s$). Hence, the time interval $\Delta\tau$ taken by such a sediment particle to vacate its space is:

$$\Delta\tau = \frac{D_{50}}{8.5u_*}. \tag{4}$$

Substituting equation 4 into equation 3 leads to the following approximate expression for the standard deviation of the noise characterizing the erosion process:

$$g_t = \frac{\delta^2}{D_{50}}\frac{8.5u_*}{1} = 8.5\frac{\delta^2}{D_{50}}u_*. \tag{5}$$

Without loss of generality, and further assuming that the smallest fluctuations in the process are of a size that is the same as the (spherical) mean sediment diameter, $\delta = D_{50}$, then equation 5 becomes:

$$g_t = 8.5D_{50}u_*, \tag{6}$$

which is the sought result.

2. Stochastic modeling of groundwater level

In order to utilize the model proposed by Tron et al. (2014), we first idealize the temporal groundwater level dynamics as a Compound Poisson Process – a convenient, robust way of representing flow variability (see e.g. Rodriguez-Iturbe et al. (1999); Bertagni et al. (2018); Calvani et al. (2019)). The Compound Poisson Process (CPP) is a synthetic signal characterized by a sequence of stochastic instantaneous pulses followed by exponential deterministic decays (Figure S2a). The CPP signal is governed by the Langevin equation that, in the case of water table dynamics, has the form:

$$\frac{dz_w}{dt} = \eta_l(h_2 - z_w) - \zeta \tag{7}$$

where z_w is the water table depth below the soil surface and h_2 is the maximum distance from the soil surface to the water table. The first term on the right-hand side of equation 7 expresses the deterministic component of the signal (exponential decay) with decay rate η_l. The second term ζ is a state variable representing the stochastic component in which pulses are modeled as white shot noise of mean rate, λ_l (Ridolfi et al., 2011), and is given by:

$$\zeta(t) = \sum_{i=1}^{\infty} h_i(t)\delta(t - t_i) \tag{8}$$

where $h_i\delta(0)$ is the amplitude of the i-th pulse at time t_i, t is time, and $\delta(\cdot)$ is the Dirac delta function. From equation 7, the steady-state probability density function of the water table level (Figure S2b) may be derived analytically (see e.g. Tron et al. (2014)) as:

$$p(z_w) = \frac{\gamma_l^{-\beta_l}}{\Gamma\left[\beta_l\right]} e^{\frac{z_w - h_2}{\gamma_l}} (h_2 - z_w)^{\beta_l - 1} \tag{9}$$

where $\Gamma[\cdot]$ is the Gamma function (Abramowitz & Stegun, 1948), γ_l is the mean amplitude of the pulses in water level, and β_l is the ratio of the mean rate of the pulses, λ_l, to η_l. Note that γ_l and β_l represent the scale and shape parameters of the PDF in Figure S2b.

In the model proposed by Tron et al. (2014), stochastic fluctuations in the water table trigger variations in water and oxygen availability in the soil, thus influencing root shape and evolution dynamics. Tron et al.'s model assumes that roots potentially grow within the zone, h_2, defined as the maximum layer thickness between the soil surface and water table depth z_w (Figure S3), below which root growth is hindered by excess water availability. Root growth is stimulated in the unsaturated zone, the so-called 'optimal root-growth zone', L, where water availability is ensured through capillary rise. This zone, whose thickness is controlled by D_{10} and D_{90} of the sediment, is located at a distance $(h_2 - h_1)$ above the water table (see Figure S3). The analytical expression of L is built on the concept of capillary rise in soil as follows:

$$L = \frac{4Tcos\zeta}{\rho g D_{10}} - \frac{4Tcos\zeta}{\rho g D_{90}} \tag{10}$$

where the first term on the right-hand side relates to the height of maximum capillary rise above the groundwater table, whereas the second term represents the thickness of the saturated capillary fringe. T is surface tension, ρ is water density, g is acceleration due to gravity and ζ is the contact angle (which is equal to 0 assuming full wettability between the rising water and the soil particles). The optimal root-growth zone L, fluctuates according to stochastic oscillation of the groundwater dynamics (Figure S3) described as a Compound Poisson Process (Figure S2a). As a result, Tron et al. (2014) assumed that the water table moves almost synchronously with the river water stage.

Root growth-decay dynamics inside and outside the zone L is modelled using dichotomous noise (Ridolfi et al., 2011). This type of noise is commonly used to describe the dynamics of systems that randomly switch between two states – in this case, root growth and death.

The equation representing root dynamics is:

$$r(z) = \frac{2\theta(z)k(z)}{\theta(z) + \theta(z)k(z) + 1 - k(z)}, \tag{11}$$

where $\theta(z)$ is the ratio of root growth rate to death rate. The function $k(z)$ expresses the probability that a generic depth below the soil surface, z, is located in the optimal root-growth zone. Hence, when a depth z is located within L, root development is enhanced; if z is located outside L, then root growth contracts because of dryness (above L) or anoxia (below L). It is hence assumed that $k(z)$ may be expressed by the following piece-wise equation:

$$k(z) = \begin{cases} \left[\Gamma\left(\beta_l, \frac{h_1 - z - L}{\gamma_l}\right) - \Gamma\left(\beta_l, \frac{h_1 - z}{\gamma_l}\right)\right] \cdot \Gamma(\beta_l)^{-1} & -\infty < z < h_1 - L \\ 1 - \Gamma\left(\beta_l, \frac{h_1 - z}{\gamma_l}\right) \cdot \Gamma(\beta_l)^{-1} & h_1 - L < z < h_1 \end{cases} \tag{12}$$

3. Scour depth L_e

Equation 4 in the main text is derived by combining models by Bau' et al. (2019) and Tron et al. (2014).

The analytical approach proposed by Bau' et al. (2019) provides a formula for calculating the critical rooting length of flexible plants at incipient uprooting. By definition, the critical rooting length corresponds to the residual rooting length of the plant when uprooting occurs and can be determined by assessing the equilibrium of forces between root resistance and flow-induced drag. Bau et al.'s model assumes that, during extreme

flow-induced erosion events, plants become reconfigured in the stream-wise direction (Figure S4b). Therefore, at incipient uprooting, the vector sum of destabilizing forces acting on the plant must balance mechanical resistance, so that:

$$\mathbf{F_n} + \mathbf{F_{d,n}} + \mathbf{F_{d,t}} = \mathbf{R}. \tag{13}$$

where $\mathbf{F_n}$ is the net buoyancy force, $\mathbf{F_{d,n}}$ is the net normal drag force, $\mathbf{F_{d,t}}$ is the net tangential drag force, and $\mathbf{R}$ is the resistance exerted by the root system.

An expression for root anchoring is particularly complicated to derive from first principles, and so it is convenient to recall empirical correlation laws derived from pullout experiments. Such laws link the resistance force $\mathbf{R}$ to the total rooting length L_r (Figure S4a):

$$\mathbf{R} = \mathbf{R}(L_r). \tag{14}$$

Consequently, the force exerted to pullout the plant $\mathbf{F_p}$ is directly related to the total rooting length L_r,

$$\mathbf{F_p} = \Phi(L_r), \tag{15}$$

where Φ is an empirical fitting relationship extracted from experimental data. Hence, equation 11 becomes:

$$\mathbf{F_n} + \mathbf{F_{d,n}} + \mathbf{F_{d,t}} = \mathbf{F_p}. \tag{16}$$

Without a priori knowledge of the total rooting length, equation 14 has to be augmented by the model of Tron et al. (2014) to determine the erosion depth L_e. The proportionality coefficient, a_m, linking root density and the total rooting length, suffices for the purpose:

$$a_m = \frac{L_r}{a_v \int_0^{z_m} r(z)dz} \tag{17}$$

where a_v accounts for the dependence between L_r and the plant species, and the integral $\int_0^{z_m} r(z)dz$ expresses the root biomass density underneath the vertical root profile $r(z)$ with depth below soil surface z_m (Figure S4a). In evaluating equation 17, we obtain L_r by recalling the balance of forces in equation 14:

$$\frac{1}{2}C_D\rho_w u^2 A_n + \frac{1}{2}C_f\rho_w u^2 A_t + \frac{1}{2}C_f\rho_w u^2 \pi d_r(L_r) = F_p(L_r) \tag{18}$$

where ρ_w is the water density, C_D is the drag coefficient, C_f is the friction coefficient, A_n is the projected area of the plant in the flow direction, A_t is the surface area of the plant subjected to the tangential component exerted by flow drag, and u is the flow velocity. With a_m evaluated and a_v assigned, the scour depth L_e is evaluated by solving the following integral:

$$L_{e,t} = a_m \int_0^{L_e} r(z)dz, \tag{19}$$

which gives the expression obtained in the main text. $L_{e,t}$ is obtained from (Figure S4b):

$$L_{e,t} = L_r - L_{c,t} \tag{20}$$

where $L_{c,t}$ is obtained in a similar way as L_r, from:

$$\frac{1}{2}C_D\rho_w u^2 A_n + \frac{1}{2}C_f\rho_w u^2 A_t + \frac{1}{2}C_f\rho_w u^2 \pi d_r(L_r - L_{c,t}) = F_p(L_{c,t}) \tag{21}$$

The calculation procedure is as follows. First, L_r is calculated from equation 17 and $L_{c,t}$ from equation 20. In certain cases, it is possible to solve these equations explicitly, depending on how the pullout law F_p is expressed. Once L_r and $L_{c,t}$ have been determined, then $L_{e,t}$ is calculated from equation 19. Finally, equation 18 is integrated numerically to obtain L_e.

4. Parameters used in the case study

A case study was undertaken for the River Maggia in Switzerland. Parameters used to implement the model for the case study are briefly described below and further summarised in Table S1.

Channel geometry and hydraulic parameters

The cross-section representative of the braided reach of the River Maggia was approximated by a trapezoidal geometry with external angle, α, of 5° and a minor base, B, of 50 m width. The channel slope was set to 5‰, which is within the range outlined by Ruf (2007). The water level in the river was computed using Engelund's method for different values of the Strickler coefficient for vegetated ($K_{s,1} = 6$) and non-vegetated ($K_{s,2} = 20$) parts of the river. The vegetated area coincides with the riverbanks, whereas the non-vegetated area comprises the channel bed. The value assigned to $K_{s,1} = 6$ corresponds to highly densely vegetated riverbanks (Hrissanthou & Kaffas, 2019).

Turning to bed-load transport, the critical Shields parameter for incipient motion, τ^*_{cr}, was set equal to 0.03 (Parker et al., 2007). Sediment porosity, λ_g was set to 0.2 according to the empirical formula suggested by Wu & Wang (2006), the exponent of the sediment transport formula, b, was given a value of 1.5 (e.g. Van Rijn's model), and the sediment-to-water density ratio, ρ_g, was set to 2600 kg/m^3. The coefficient of the bed-load transport formula, α_{BL}, was set equal to 3.97, following Wong & Parker (2006). A representative value for ΔX proved difficult to assign, and so, following Calvani et al. (2019), ΔX was assumed equal to $6B$, which is approximately the length scale of a bar according to Leopold & Wolman (1957).

Soil texture parameters

The grain size distribution of riverbank soil is unknown for the River Maggia in Valle Maggia, Switzerland. Hence, values assigned to D_{10} and D_{90} are purely indicative. Furthermore, given the sediment retention capacity of the dam, it is appropriate to account for a shift in sediment size between the pre- and post-dam periods. The change in sediment supply and the resulting decrease in bed mobility downstream of the dam lead to the intuitive assumption that sediment size increased in the post-dam period.

In the case study, D_{90} and D_{10} of the riverbank soil were prescribed to vary from 0.12 to 0.24 mm and from 0.03 to 0.06 mm between the two states. For the riverbed sediment grain size distribution, Ruf (2007) suggested the median value for riverbed pebbles, D_{50}, was about 100 mm. The value of D_{50} in the pre-dam scenario was taken equal to 65 mm, noting that the actual value is unknown.

Vegetation properties

We assumed the pullout law followed a polynomial trend (i.e. $F_p(L_r)$=$0.025L_r + 0.6L_r$), appropriate for plants at an advanced stage of growth (Edmaier et al., 2014). For the sake of simplicity, the coefficient a_v was set equal to 1 so as to consider plants with the same allometric relationships between below- and above-ground biomass. The drag coefficient, C_D, was assigned a representative value of 1.0, in accordance with Bau' et al. (2019). The friction coefficient value of $C_f = 3$ was higher than that calibrated by Bau' et al. (2019). This was because of the more complicated plant geometry, comprising a larger number of branches and leaves and more complex configuration (Järvelä, 2002). The surface area of the plant exposed to flow, A_t, was prescribed as 1 m^2, whereas the projected area of the

stem and branches in the flow direction, A_n, was set to 0.5 m^2. The mean diameter of a single root was assumed to be 3 x 10^{-3} m.

Note that the free-body model has been applied without revisiting its inherent assumptions for two reasons. First, there are no input values for the plant properties. Second, plants likely to be uprooted are usually still in their intermediate stage of growth (thus flexible). It should also be noted that species differences and growth stage dynamics of vegetation are not explicitly included in the model. Therefore, the maximum depth that the root can reach, z_m, is not constrained by vegetation type and age, and solely depends on plant elevation, soil texture, and water table level.

5. Sensitivity Analysis

We performed a sensitivity analysis for the two most important input parameters: plant elevation, and grain size distribution of the riverbank soil.

Figure S5 shows equilibrium curves obtained for a plant of elevation varying between 0.8 to 2 m, and constant values of D_{10} and D_{90} between the pre- and post-dam periods. For comparison purposes, uprooting probability was plotted against the non-dimensional ratio $\Delta\tilde{H}$, defined as $\Delta\tilde{H} = \frac{\Delta H}{\eta_v}$ where ΔH is the difference between plant soil elevation and mean water stage and η_v is the plant elevation.

Role of plant elevation

From Figure S5a it is evident that, at the state points P1 and P3, uprooting probability decreases as plant elevation increases and vice versa. This is quite intuitive for the post-dam period, when plants located closest to the riverbed are more likely to be uprooted given the long periods of low flow conditions. Conversely, plants at higher elevation are

only inundated during sporadic flood events that cannot be contained by the dam (see Figure 2b1 in the main text). The same logic can be applied to the pre-dam period, where plants with higher probability of being stressed by drag forces are also inundated during low flow conditions in winter.

Figure S6a presents the variation in probability of plant uprooting with plant elevation on the riverbank. Figure S6a is particularly useful in illustrating to what extent the elevation of the plant influences the uprooting percentage at points P1, P2, P3, and P4. Uprooting percentages at P1 and P3 decrease as the plant elevation increases. The uprooting percentage at P3 decreases more rapidly with plant elevation than at the pre-dam point P1. Hence, the low flow conditions of the post-dam scenario have greater impact on uprooting probability.

Figures S6b, S6c, and S6d illustrate differences in uprooting percentage, ΔP_τ, obtained between the points P1 & P3, P2 & P3, and P1 & P4, as functions of plant elevation. The trends appear parabolic, and are remarkably similar, each with a maximum at η_v between 1.2 and 1.5. Plants at different elevations therefore display the same response in terms of ecosystem shift (Figure S6b), adaptation to post-dam equilibrium (Figure S6c), and ability to re-establish pre-dam conditions (Figure S6d). However, it is important to note that these seemingly similar reactions by plants at different elevations have different causes. This can be seen, for instance, by comparing Figure S6b with Figure S6a. For plants located at elevations lower than 1.3 m, the uprooting probability at P3 decreases much more rapidly than at P1. The opposite is observed in the trend of the uprooting probability for plants at elevations between 1.4 and 1.7 m, where rapid decrease in P_τ occurs at P1.

Role of soil parameters

Figure S5b replots the same curves as Figure S5a, the only difference being that, in this case, the values assigned to D_{10} and D_{90} are kept constant between P1 and P3. In other words, this is a scenario that would occur if the dam had no impact on downstream sediment supply. Although not a natural scenario, this could occur if sediment continuity was artificially maintained. Figure S5b shows that such change could significantly affect the uprooting probability. Specifically, P_τ reaches higher values during the post-dam period than in Figures S5a for the same plant elevations. Trends in P_τ at P1 and at P2 (Figure S7a) are almost the same as those represented in Figure S6a. However, this is not the case at P3 and P4.

Comparison between Figure S7 and Figure S6 reveals that maintaining D_{10} and D_{90} constant mostly affects the uprooting probability of plants whose elevation is less than about 1.5 m. By maintaining the same soil texture between P1 and P3, the retention capacity of the soil remains unchanged as well. Hence, compared to the results in Figures S5a and S6, at P3 the roots do not have to propagate to deeper layers in order to reach the water table. This implies that plants can reach the equilibrium point at P3, and approach P4 more easily. However, this finding does not also apply to plants that grow at higher elevations, where ΔP_τ appears almost independent of soil texture (compare Figures S7a and S7b to Figures S6a and S6b).

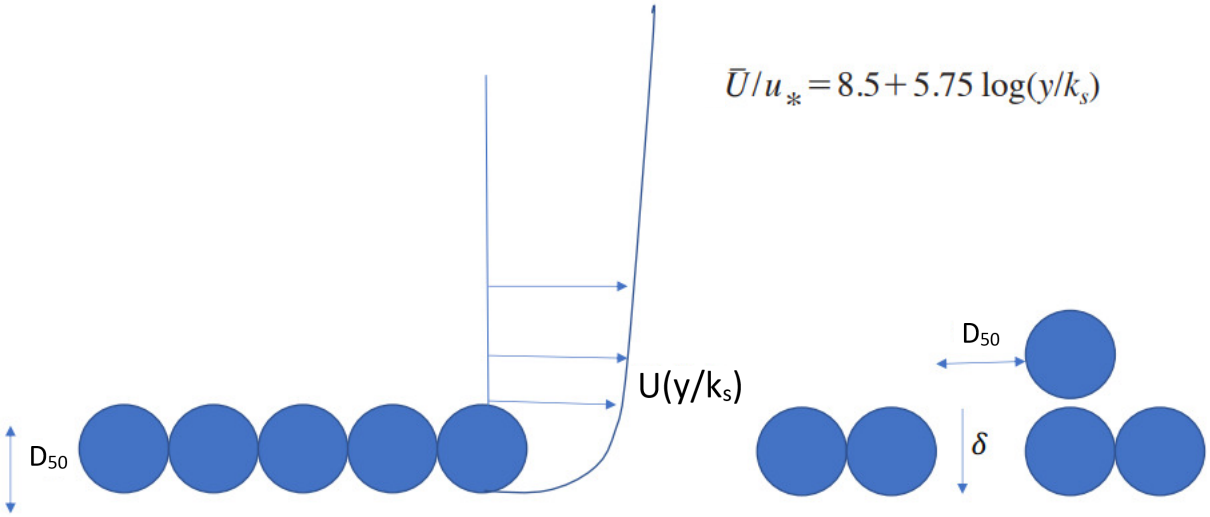

Figure S1. Longitudinal velocity profile of a particle, and similarity between the spatial scale of the particle and its median size D_{50}.

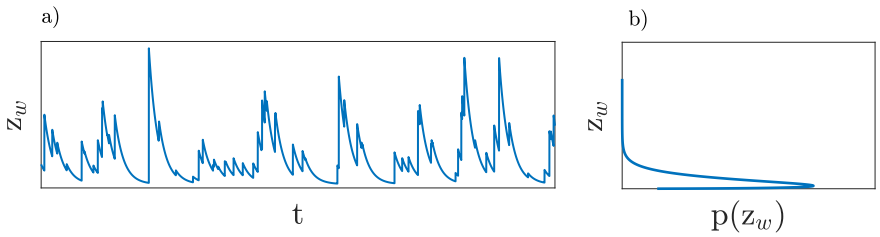

Figure S2. Stochastic dynamics of groundwater level: a) simulated Compound Poisson Process for water table level, z_w; and b) probability density function of water table level, $p(z_w)$.

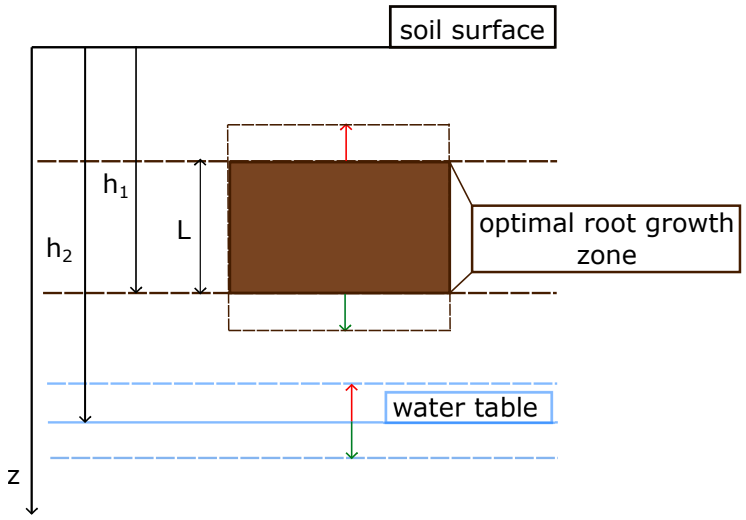

Figure S3. Sketch depicting synchronous fluctuations in groundwater level and the optimal root-growth zone L. Oscillations are indicated by dashed lines: rising in red, falling in green.

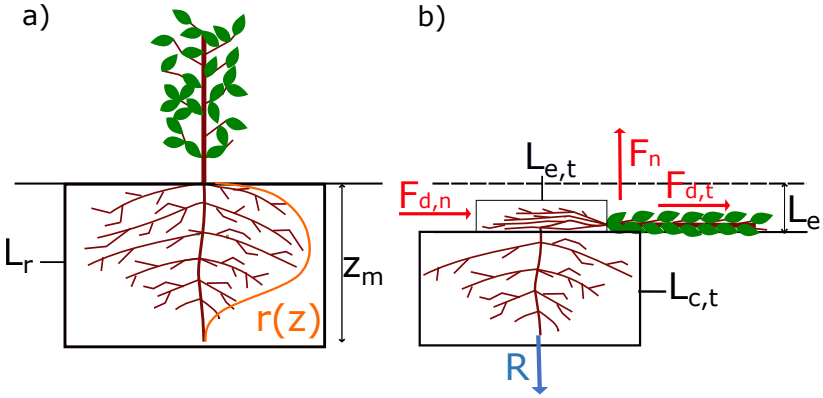

Figure S4. Outline of the free-body model. a) Upright plant without bed erosion (L_e = 0). Total length of below-ground biomass is L_r, whose density is represented by the integral of the analytical root profile $r(z)$ between the soil surface and the rooting depth z_m. b) Forces acting on a bent plant (red coloured arrows) and root mechanical resistance (blue coloured arrow) at the uprooting time. Due to scouring around the plant, part of the root system is partially exposed ($L_{e,t}$), hence reducing the rooting length to $L_{c,t}$.

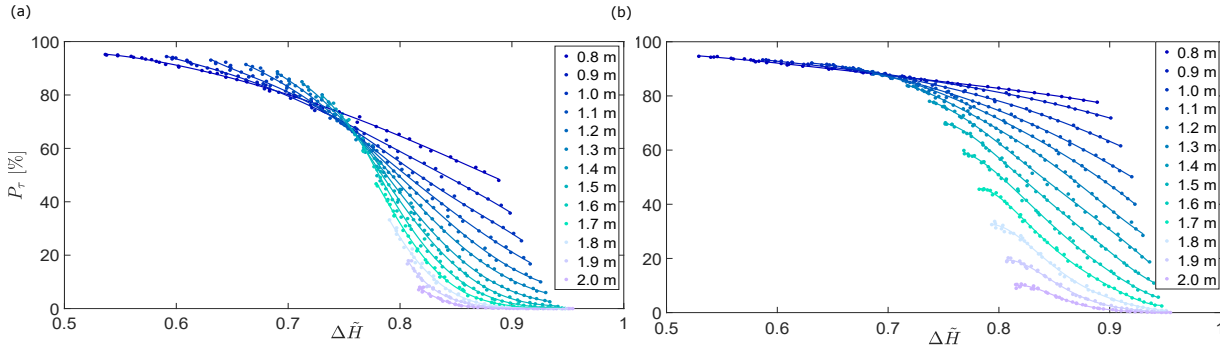

Figure S5. Uprooting probability, P_τ, plotted against the ratio of the difference between plant soil elevation and mean water stage to the plant elevation, $\Delta\tilde{H}$, for a) a range of plant elevations between 0.8 and 2 m b) and for constant values of D_{10} and D_{90}.

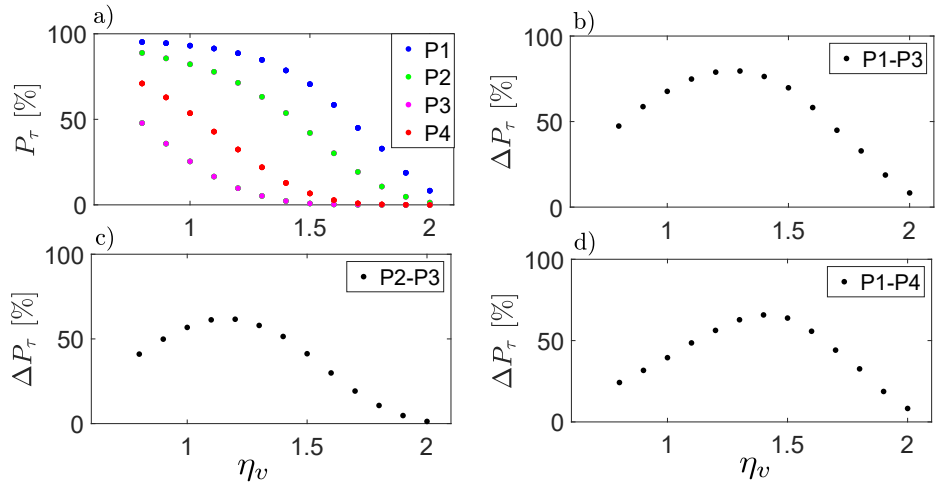

Figure S6. a) Variation in uprooting probability P_τ with plant elevation on the riverbank at P1, P2, P3, and P4. b)-d) Variation in difference in the uprooting probability with plant elevation on the riverbank for different values of η_v between: b) P1 & P3, c) P2 & P3, d) P1 & P4.

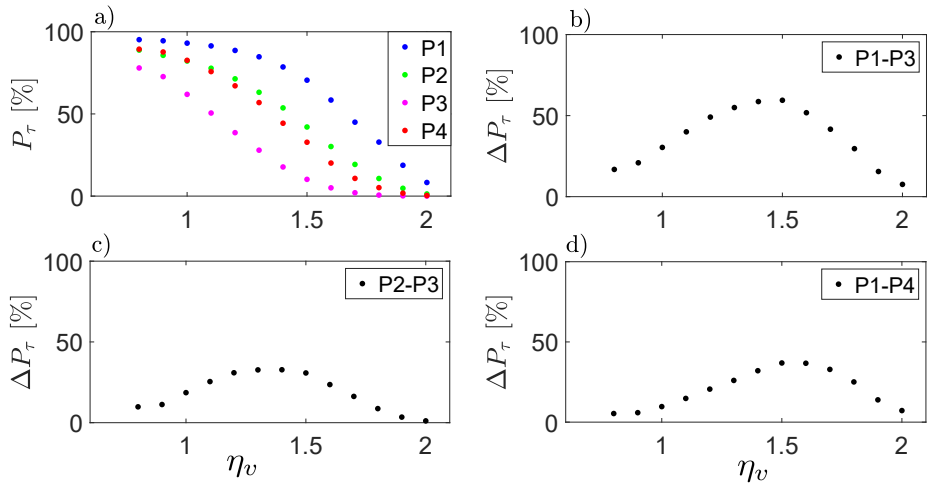

Figure S7. a) Variation in uprooting probability P_τ with plant elevation on the riverbank at states P1, P2, P3, and P4, while keeping the value of soil texture constant between P1 and P3. b)-d) Variation in difference in uprooting probability with plant elevation on the riverbank for different values of η_v and constant values of D_{10} and D_{90} between: b) P1 & P3, c) P2 & P3, d) P1 & P4.

Table S1. Input data to the model.

Input parameters	description	pre-dam	post-dam
τ_d	integral temporal scale	3.31 d	1.60 d
γ_d	average jump height	23 m^3s^{-1}	50 m^3s^{-1}
λ_d	average jump height	0.22 d^{-1}	0.05 d^{-1}
B	river width	50 m	50 m
$K_{s,1}$	river bed Strickler coefficient	20 $m^{1/3}s^{-1}$	20 $m^{1/3}s^{-1}$
$K_{s,2}$	vegetation Strickler coefficient	6 $m^{1/3}s^{-1}$	6 $m^{1/3}s^{-1}$
S	river slope	5‰	5‰
ρ_g	sediment density	2600 kgm^{-3}	2600 kgm^{-3}
λ_g	sediment porosity	0.2	0.2
b	exponent in sediment transport formula	1.5	1.5
ΔX	longitudinal length scale of bed erosion	300 m	300 m
α_{BL}	coefficient in bedload transport formula	3.97	3.97
τ^*_{cr}	critical Shields parameter	0.03	0.03
g_t	erosion process noise	0.18 m^2 d^{-1}	0.18 m^2 d^{-1}
D_{10}	grain size value	3.4 x 10^{-5} m	6.0 x 10^{-5} m
D_{90}	grain size value	1.2 x 10^{-4} m	2.4 x 10^{-4} m
D_{50}	median pebble size	6.5 x 10^{-2} m	1.0 x 10^{-1} m
C_d	drag coefficient	1.0	1.0
C_f	friction coefficient	3.0	3.0
d_r	root diameter	3 x 10^{-3} m	3 x 10^{-3} m
A_t	plant surface area	1 m^2	1 m^2
A_n	plant normal area	5 x 10^{-1} m^2	5 x 10^{-1} m^2
η_v	plant elevation	1.2 m	1.2 m
a_v	coefficient of plant species	1.0	1.0
a_r	coefficient of pullout law†	0.025	0.025
b_r	coefficient of pullout law†	0.6	0.6

† static pullout law: $F_p = a_r x^2 + b_r x$

References

Abramowitz, M., & Stegun, I. A. (1948). *Handbook of mathematical functions with formulas, graphs, and mathematical tables* (Vol. 55). US Government printing office.

Bau', V., Zen, S., Calvani, G., & Perona, P. (2019). Extracting the critical rooting length in plant uprooting by flow from pullout experiments. *Water Resources Research*.

Bertagni, M. B., Perona, P., & Camporeale, C. (2018). Parametric transitions between bare and vegetated states in water-driven patterns. *Proceedings of the National Academy of Sciences*, *115*(32), 8125–8130.

Calvani, G., Perona, P., Zen, S., Bau', V., & Solari, L. (2019). Return period of vegetation uprooting by flow. *Journal of Hydrology*, *578*, 124103.

Edmaier, K., Crouzy, B., Ennos, R., Burlando, P., & Perona, P. (2014). Influence of root characteristics and soil variables on the uprooting mechanics of Avena sativa and Medicago sativa seedlings. *Earth Surface Processes and Landforms*, *39*(10), 1354–1364.

Einstein, A. (1905). Über die von der molekularkinetischen Theorie der Wärme geforderte Bewegung von in ruhenden Flüssigkeiten suspendierten Teilchen. *Annalen der Physik*, *322*(8), 549-560.

Hrissanthou, V., & Kaffas, K. (2019). *Soil erosion: Rainfall erosivity and risk assessment*. IntechOpen.

Järvelä, J. (2002). Determination of flow resistance of vegetated channel banks and floodplains. In B. . Zech (Ed.), *River flow 2002* (pp. 311–318). Swets & Zeitlinger, Lisse.

Leopold, L. B., & Wolman, M. G. (1957). *River channel patterns: braided, meandering, and straight*. US Government Printing Office.

Papanicolaou, A., Diplas, P., Evaggelopoulos, N., & Fotopoulos, S. (2002). Stochastic incipi-

ent motion criterion for spheres under various bed packing conditions. *Journal of Hydraulic Engineering*, *128*(4), 369–380.

Parker, G., Wilcock, P. R., Paola, C., Dietrich, W. E., & Pitlick, J. (2007). Physical basis for quasi-universal relations describing bankfull hydraulic geometry of single-thread gravel bed rivers. *Journal of Geophysical Research: Earth Surface*, *112*(F4).

Perona, P., & Crouzy, B. (2018). Resilience of riverbed vegetation to uprooting by flow. *Proceedings of the Royal Society A: Mathematical, Physical and Engineering Sciences*, *474*(2211), 20170547.

Ridolfi, L., D'Odorico, P., & Laio, F. (2011). *Noise-induced phenomena in the environmental sciences*. Cambridge University Press.

Rodriguez-Iturbe, I., Porporato, A., Ridolfi, L., Isham, V., & Cox, D. (1999). Probabilistic modelling of water balance at a point: the role of climate, soil and vegetation. *Proc. R. Soc. Lond. A*, *455*, 3789-3805.

Ruf, W. (2007). *Numerical modelling of distributed river: aquifer coupling in an alpine floodplain* (Ph.D. thesis). ETH Zurich.

Tron, S., Laio, F., & Ridolfi, L. (2014). Effect of water table fluctuations on phreatophytic root distribution. *Journal of Theoretical Biology*, *360*, 102–108.

Uhlenbeck, G. E., & Ornstein, L. S. (1930). On the theory of the Brownian motion. *Physical review*, *36*(5), 823.

Wong, M., & Parker, G. (2006). Reanalysis and correction of bed-load relation of meyer-peter and müller using their own database. *Journal of Hydraulic Engineering*, *132*(11), 1159–1168.

Wu, W., & Wang, S. S. (2006). Formulas for sediment porosity and settling velocity. *Journal of Hydraulic Engineering*, *132*(8), 858–862.